RESEARCH ARTICLE SUMMARY

STRUCTURAL BIOLOGY

Structural basis for the recognition of Sonic Hedgehog by human Patched1

Xin Gong*, Hongwu Qian*, Pingping Cao*, Xin Zhao, Qiang Zhou, Jianlin Lei, Nieng Yan†

INTRODUCTION: The Hedgehog (Hh) pathway is critical for embryogenesis and tissue regeneration. Hh signaling is activated by binding of the secreted and lipid-modified protein Hh to the membrane receptor Patched (Ptch). In the absence of Hh, Ptch suppresses the downstream G protein–coupled receptor Smoothened (Smo) via an unknown and indirect mechanism. Binding of Hh to Ptch relieves the inhibition on Smo and turns on the signaling events that lead to the transcriptional activation of the Hh pathway. Aberrations of Hh signaling are associated with birth defects or tumorigenesis. Despite rigorous investigations, the molecular basis for the interplay among Hh, Ptch, and Smo remains unclear, and the structural basis for the recognition between Ptch and Hh is yet to be elucidated.

The 1447-residue human Ptch1 protein is predicted to contain 12 transmembrane segments (TMs) and to share structural similarity with the bacterial resistance-nodulation-division (RND) family transporters. TMs 2 to 6 of Ptch1 constitute the sterol-sensing domain (SSD), which has been found in several proteins involved in sterol transport and metabolism. The molecular mechanism for potential sterol binding or transport activity of these SSD-containing proteins remains elusive.

RATIONALE: To obtain a sample suitable for structural study, we generated several constructs of human Ptch1 based on sequence conservation and functional characterizations. Eventually, the truncated human Ptch1 containing residues 1 to 1305, which was transiently expressed in human embryonic kidney (HEK) 293F cells, exhibited a sufficient expression level and good solution behavior after affinity and size exclusion chromatography purification. Both oligomeric and monomeric states of Ptch1 were observed. The monomeric form was used for single-particle cryo–electron microscopy (cryo-EM) analysis because of its excellent behavior under cryo conditions.

ON OUR WEBSITE

Read the full article at http://dx.doi.org/10.1126/science.aas8935

Among the three mammalian Hh homologs Sonic (Shh), Desert (Dhh), and Indian (Ihh), Shh has been the prototype for functional and mechanistic investigations. The N-terminal domain of human Sonic Hh (ShhN, residues 24 to 197) expressed and purified in *Escherichia coli* was able to form a stable complex with the detergent-solubilized Ptch1 protein in the presence of cholesteryl hemisuccinate (CHS).

RESULTS: The cryo-EM structures of human Ptch1 alone and in complex with ShhN were determined at overall resolutions of 3.9 Å and 3.6 Å, respectively. Two interacting extracellular domains, ECD1 and ECD2, and 12 TMs are resolved for Ptch1. ECD1 and ECD2 move toward each other upon arrival of ShhN and together constitute the docking site for ShhN. Detailed recognition between ShhN and Ptch1 was analyzed and biochemically confirmed.

Two elongated densities, both consistent with CHS, are observed in Ptch1 with or without ShhN, one in a pocket enclosed by the ECD domains and the other in a membrane-facing cavity of the SSD. Structure-guided biochemical analyses revealed steroid-dependent interaction between ShhN and Ptch1. The structure of a steroid binding–deficient Ptch1 mutant displays pronounced conformational rearrangements relative to the wild-type protein.

CONCLUSION: The structures of human Ptch1 and its complex with ShhN reveal the molecular basis for the recognition between Ptch1 and ShhN. The identification of two steroid-binding sites in Ptch1 establishes an important framework for future investigations of Hh signaling and provides critical insight into sterol perception by SSD-containing proteins. ■

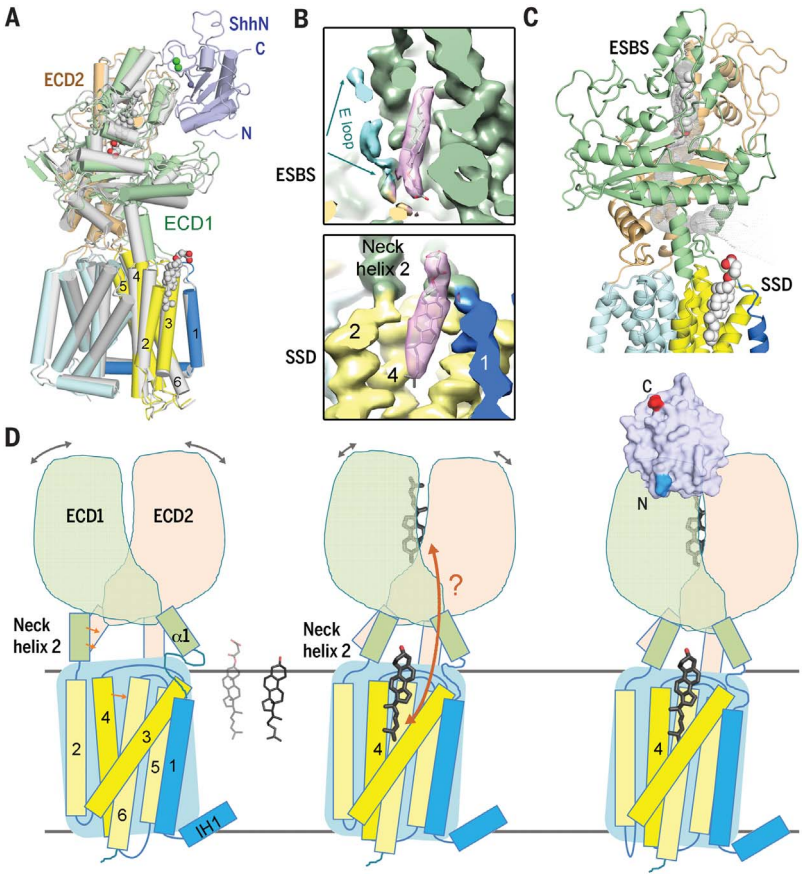

Structural basis for sterol perception by the sterol-sensing domain (SSD) and steroid-dependent binding between Ptch1 and ShhN. (**A**) Structural comparison of Ptch1 alone (silver) and in complex with ShhN (domain-colored). (**B**) Two CHS binding sites on Ptch1, one enclosed by extracellular domains [the extracellular steroid binding site (ESBS)] and one on the SSD. (**C**) Potential sterol transfer between the two binding sites. (**D**) Functional implications of the structures.

The list of author affiliations is available in the full article online.
*These authors contributed equally to this work.
†Corresponding author. Email: nyan@princeton.edu
Cite this article as X. Gong *et al.*, *Science* **361**, eaas8935 (2018). DOI: 10.1126/science.aas8935

RESEARCH ARTICLE

STRUCTURAL BIOLOGY

Structural basis for the recognition of Sonic Hedgehog by human Patched1

Xin Gong[1]*†, Hongwu Qian[1]*†, Pingping Cao[1]†, Xin Zhao[1], Qiang Zhou[1], Jianlin Lei[2], Nieng Yan[1]*‡

The Hedgehog (Hh) pathway involved in development and regeneration is activated by the extracellular binding of Hh to the membrane receptor Patched (Ptch). We report the structures of human Ptch1 alone and in complex with the N-terminal domain of human Sonic hedgehog (ShhN) at resolutions of 3.9 and 3.6 angstroms, respectively, as determined by cryo–electron microscopy. Ptch1 comprises two interacting extracellular domains, ECD1 and ECD2, and 12 transmembrane segments (TMs), with TMs 2 to 6 constituting the sterol-sensing domain (SSD). Two steroid-shaped densities are resolved in both structures, one enclosed by ECD1/2 and the other in the membrane-facing cavity of the SSD. Structure-guided mutational analysis shows that interaction between ShhN and Ptch1 is steroid-dependent. The structure of a steroid binding–deficient Ptch1 mutant displays pronounced conformational rearrangements.

The Hedgehog (Hh) signaling pathway, which has been investigated extensively in *Drosophila* and vertebrates, plays a pivotal role in embryogenesis and postnatal tissue maintenance and regeneration (*1*–*5*). Activation of Hh signaling is initiated by binding of the secreted protein Hh to the membrane-embedded receptor Patched (Ptch) in Hh-responsive cells (*6*–*8*). In the absence of Hh, Ptch inhibits Smoothened (Smo), a class F GPCR (G protein–coupled receptor), although the mechanism remains unclear (*9*–*11*). Binding of Hh to Ptch relieves the inhibition on Smo and turns on the signaling events that lead to the transcriptional activation of the Hh pathway (*12*–*17*). Compromised Hh pathway activity may result in birth defects, whereas aberrant activation of Hh signaling by suppressing Ptch or activating Smo has been implicated in tumorigenesis of several tissues, as exemplified by basal cell carcinoma and medulloblastoma (*18*–*22*).

In mammals, three Hh homologs have been identified—Sonic (Shh), Desert (Dhh), and Indian (Ihh)—among which Shh represents the prototype for functional and mechanistic elucidation (*5*). A ~450-residue Shh precursor undergoes autocatalytic cleavage and yields an N-terminal domain (ShhN) of ~20 kDa that is responsible for all known signaling activities. ShhN is modified with N-terminal palmitoyl and C-terminal cholesteryl moieties (*23*–*27*). Although unpalmitoylated ShhN exhibits decreased activity (*26*, *28*), these modifications are dispensable for the high-affinity binding to Ptch (*29*).

Because abnormal activation of the Hh pathway is associated with tumorigenesis, different types of inhibitors have been developed that target Hh signaling (*30*, *31*) (fig. S1). Most of these are antagonists for Smo or inhibitors of downstream components in the Hh pathway. However, some of them are designed to disrupt the interaction between Ptch1 and ShhN, such as Robotnikinin (*32*) and HL2-m5 macrocyclic peptide (*33*) (fig. S1). Structural information on the ShhN-Ptch1 complex may provide important insight into design or optimization of ligands to disrupt the formation of a complex between ShhN and Ptch1. Whereas a number of crystal structures of ShhN segments alone and in complex with different binding proteins have been reported (*34*), there has been a lack of structural information on Ptch.

Patched (*ptc*) was cloned as a segment-patterning gene in *Drosophila* (*35*, *36*). The human homolog was later identified as a tumor suppressor for basal cell nevus syndrome (also known as Gorlin syndrome) (*37*, *38*). There are two Ptch homologs in mammals, Ptch1 and Ptch2, both of which, despite their divergent expression patterns and physiological functions, bind to the three types of mammalian Hh ligands with similar affinity (*39*, *40*). The full-length human Ptch1 (hPtch1), consisting of 1447 amino acids, is predicted to contain 12 transmembrane segments (TMs), two extracellular domains (ECDs), and two intracellular domains (*37*). Ptch proteins share sequence similarity with the bacterial resistance-nodulation-division (RND) family transporters exemplified by the proton-driven multidrug resistance pump AcrB (*41*, *42*). TMs 2 to 6 of Ptch constitute the sterol-sensing domain (SSD) that has been found in a number of sterol transport and metabolism-related proteins, such as 3-hydroxy-3-methylglutaryl–coenzyme A reductase (HMGCR), SREBP cleavage-activating protein (SCAP), Niemann-Pick type C1 (NPC1), NPC1-like 1 (NPC1L1), and another Hh signaling component, Dispatched (Disp) (*43*). Although the structures of human NPC1 have recently been determined, the molecular mechanism of potential sterol binding or transport mediated by the SSD-containing proteins remains enigmatic (*44*, *45*).

Here, we report the cryo–electron microscopy (cryo-EM) structures of human Ptch1 alone and in complex with ShhN at overall resolutions of 3.9 Å and 3.6 Å, respectively. The structures reveal the detailed recognition between ShhN and Ptch1. Unexpectedly, two steroid molecules are observed, one in a pocket enclosed by the ECDs and one in the membrane-facing cavity of the SSD. Structure-guided biochemical analyses suggest that the interaction between ShhN and Ptch1 is steroid-dependent—an observation corroborated by additional structural evidence.

Structural determination of human Ptch1 and the Ptch1-ShhN complex

To obtain a sample suitable for structural study, we generated several constructs of human Ptch1 based on sequence conservation and functional characterizations (fig. S2) (*8*, *46*, *47*). Consistent with a previous observation in a cell-based binding assay that the C terminus–truncated mouse Ptch1 binds to ShhN with affinity similar to that of wild-type Ptch1 (Ptch1-WT) (*8*), the C terminal intracellular domain of mouse Ptch1 was shown to be dispensable for Ptch1-dependent regulation of canonical Hh signaling (*46*, *47*). We therefore tested a number of C-terminus truncations and identified an optimal construct for human Ptch1 (residues 1 to 1305) that exhibited sufficient expression level and good solution behavior (fig. S3). [See below for details of the subcloning, transient human embryonic kidney (HEK) 293F cell expression, purification, and cryo-EM data acquisition of Ptch1.]

Consistent with the reported oligomerization of Ptch1 (*47*, *48*), recombinant Ptch1 eluted in two peaks upon size-exclusion chromatography (SEC), suggesting distinct oligomerization states (fig. S3B). Preliminary assessment using cryo-EM showed that protein particles in the earlier peak were heterogeneous, posing a major challenge for structural determination. In contrast, the proteins in the later peak, despite its smaller size, appeared homogeneous and displayed multiple orientations in the thin layer of vitreous ice. We therefore focused on the monomeric form of Ptch1 for cryo-EM analysis.

An EM reconstruction was obtained at 3.9 Å resolution from 94,445 selected particles (fig. S3C) according to the gold-standard Fourier shell correlation 0.143 criterion. Although the construct used for structural determination contains 1305 residues, all the intracellular segments—including the 72 residues on the N terminus, residues 608 to 730 that connect TMD1 (TMs 1 to 6)

[1]State Key Laboratory of Membrane Biology, Beijing Advanced Innovation Center for Structural Biology, Tsinghua-Peking Joint Center for Life Sciences, School of Life Sciences and School of Medicine, Tsinghua University, Beijing 100084, China. [2]Technology Center for Protein Sciences, Ministry of Education Key Laboratory of Protein Sciences, School of Life Sciences, Tsinghua University, Beijing 100084, China.
*Present address: Department of Molecular Biology, Princeton University, Princeton, NJ 08544, USA. †These authors contributed equally to this work.
‡Corresponding author. Email: nyan@princeton.edu

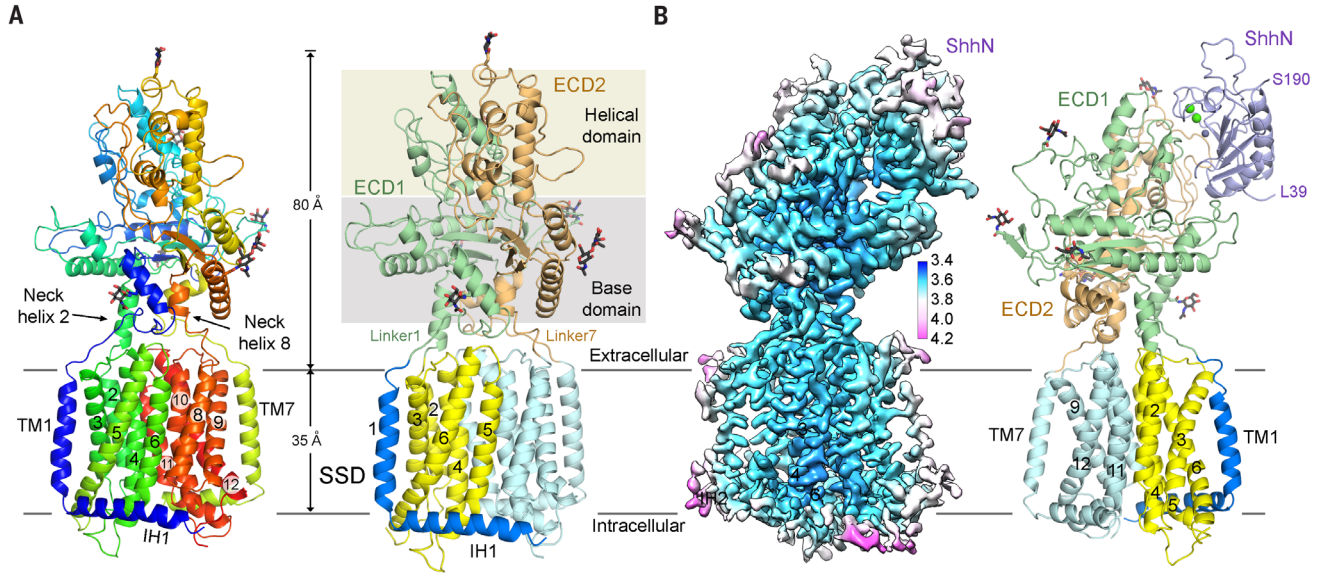

Fig. 1. Cryo-EM structures of human Patched1 (Ptch1) alone and in complex with ShhN. (**A**) Overall structure of Ptch1. The structures shown on the left and right are rainbow and domain-colored, respectively. The sterol-sensing domain (SSD) that consists of TMs 2 to 6 is colored yellow. The sugar moieties are shown as sticks. See fig. S7 for the detailed structural illustration of individual domains. Unless otherwise indicated, the same color code is applied to all figures. (**B**) Structure of Ptch1 in complex with ShhN. Left: The resolution map for the Ptch1-ShhN complex. The color code for resolutions, shown with the unit Å, is calculated using Relion 2.0 (*73*) and generated in Chimera (*80*). Right: Overall structure of the Ptch1-ShhN complex. The Ca^{2+} and Zn^{2+} ions are shown as green and purple spheres, respectively. All structure figures were prepared using PyMol (*81*).

and TMD2 (TMs 7 to 12), and the C-terminal segment after Ser^{1185}—are invisible, likely owing to intrinsic flexibility. In total, 990 residues were built with 969 side chains assigned (Fig. 1A, Table 1, and figs. S4A, S5A, and S6A).

The well-resolved regions include two ECDs and the 12 TMs that display a typical RND family architecture with a two-fold pseudosymmetry around an axis that is perpendicular to the membrane (Fig. 1A and fig. S7A) (*44*, *49*). The two TMDs, each preceded by an amphiphilic helix that lies on the intracellular boundary of the membrane (designated IH), can be superimposed with a root mean square deviation (RMSD) of 3.7 Å over 186 Cα atoms (fig. S7B).

The two ECDs in Ptch1, ECD1 between TM1 and TM2 and ECD2 between TM7 and TM8, correspond to domain C and domain I in NPC1, respectively (*44*). Each ECD is linked to the N-terminal TM by a long linker (linker 1 for ECD1 and linker 7 for ECD2) and to the C-terminal TM by a Neck helix (Fig. 1A and fig. S7C). ECD1 and ECD2 both contain a topologically similar core region right above the TMD, which we term the "base domain" (Fig. 1A and fig. S7, C and D). Despite similar folds of the two base domains, ECD1 and ECD2 display divergent spatial arrangements and cannot be well superimposed (fig. S7D).

On top of the base domains, ECD1 and ECD2 each contain an extra helical domain that is absent in NPC1 (Fig. 1A). Notably, both ECDs are enriched in lengthy loops (fig. S7C). For instance, the segment (residues 943 to 969) that connects β2 and β3 in the base domain of ECD2 forms an upward-extending loop hairpin (designated the H loop) that represents part of the helical domain (figs. S2 and S7, A and C). The two ECDs interact with each other through an extended

Table 1. Summary of data collection and model statistics.

Data collection	Ptch1-WT	Ptch1-ShhN	Ptch1-3M
EM		Titan Krios (Thermo Fisher)	
Voltage (kV)		300	
Detector		K2 Summit (Gatan)	
Pixel size (Å/pixel)		1.091	
Electron dose (e^-/Å^2)		50	
Number of micrographs	3983	4221	6680
Reconstruction			
Software		RELION 2.0	
Number of used particles	94,445	137,823	154,721
Symmetry		C1	
Resolution	3.9 Å	3.6 Å	4.1 Å
Map sharpening *B*-factor (Å^2)	–170	–130	–197
Model building			
Software		COOT	
Refinement			
Software		Phenix	
Model composition			
Protein residues	990	1144	982
Side chain	969	1132	969
Sugar moieties	7	7	7
Ligands	2	2	0
Metal ions	0	3	0
Validation			
RMS deviations			
Bond length (Å)	0.01	0.01	0.01
Bond angle (degrees)	1.55	1.61	1.47
Ramachandran plot statistics (%)			
Preferred	86.21	87.42	88.63
Allowed	13.18	11.61	11.07
Outlier	0.61	0.97	0.31

yet loose interface and both project into the extracellular space with similar heights of approximately 80 Å (Fig. 1A). Six glycosylation sites were observed, four on ECD1 and two on ECD2 (fig. S7C).

For structural determination of the complex between Ptch1 and ShhN, we overexpressed human ShhN (residues 24 to 197) in *Escherichia coli* and incubated the purified protein with the C terminus–truncated human Ptch1 for cryo-EM analysis. (See below for details of the reconstitution, sample preparation, and cryo-EM data acquisition of the Ptch1-ShhN complex.) A total of 137,823 selected particles yielded a reconstruction at 3.6 Å resolution, which contains density for ShhN (Fig. 1B, Table 1, and figs. S4B and S5B). The crystal structure of ShhN (PDB code 4C4M) was docked into the density with manual adjustment. Residues 39 to 190 of ShhN were resolved (Fig. 1B). The improved resolution allows more accurate structural modeling of Ptch1 (Fig. 1B and fig. S6, B and C). Most of the structural descriptions hereafter are based on the complex structure if not otherwise noted.

Interface between Ptch1 and ShhN

ShhN binds to the Ptch1 surface constituted by the upper helical domains of the two ECDs (Fig. 2A). An extended loop (residues 206 to 213) on ECD1 designated the E loop (because it contains the conserved Glu^{212}) (fig. S2), the ensuing helix α3 on ECD1, and the H loop on ECD2 constitute the primary binding site for ShhN (Fig. 2A).

In addition to Ptch and Smo, Hh signaling is subject to regulation by cell surface or extracellular proteins, such as the co-receptors Cdon/Boc (equivalent of Ihog/Boi in invertebrates), the extracellular Hh antagonist Hhip (Hh interacting protein), and the antagonist antibody 5E1 (*34*). ShhN, which shares structural homology to a bacterial carboxypeptidase but lacks hydrolytic activity, contains a Lys/Arg-enriched pseudo–active site groove that represents the primary surface for many binding proteins (*8*). Examination of the structure of the Ptch1-ShhN complex reveals that the Ptch1-interacting surface, which involves the pseudo–active site groove, overlaps with that for other binding proteins, including the FNIII repeat of Cdo (CdoFn3), Hhip, and 5E1 Fab (fig. S8). The structure thus provides the basis for the observed competitive binding for Hh by Ptch1 and several binding proteins (*50*–*53*).

The ShhN-Ptch1 interface is primarily mediated by polar and charged residues (Fig. 2B). ECD1 and ECD2 each contribute multiple acidic residues for interaction with the Lys/Arg patch that lines the pseudo–active site groove of ShhN. The reported resolution for the interface is approximately 3.8 Å (Fig. 1B), insufficient for accurate distance measurement between atoms that may form electrostatic interactions. Nonetheless, the backbones are well defined, supporting analysis of the interface residues. Glu^{212} on the E loop of ECD1 appears to be a coordination center, interacting with Lys^{87}, Arg^{123}, and Arg^{153} on ShhN. Glu^{221} on helix α3 interacts with Tyr^{44} and Lys^{45} of ShhN, and the preceding Asp^{217} is hydrogen-bonded to Ser^{177} (Fig. 2B, left). ECD2 mainly engages Glu^{947}, Asp^{951}, Asp^{954}, and Glu^{958} on the H loop for ShhN binding (Fig. 2B, right).

The structural observation was verified by mutational analysis. We used wild-type or mutated ShhN proteins that were fused to MBP as bait to pull down Ptch1 variants (Fig. 2C). Single point mutations of the aforementioned ShhN or Ptch1 residues to opposite charges or double mutations to Ala all resulted in compromised complex formation. As a control, Ala substitution of ShhN-Thr^{77} (T77A), which is not engaged in Ptch1 interactions, had no effect on Ptch1 binding (Fig. 2C).

An extracellular steroid-binding site in Ptch1

Structural comparison of Ptch1 in the absence and presence of ShhN reveals marked shifts of

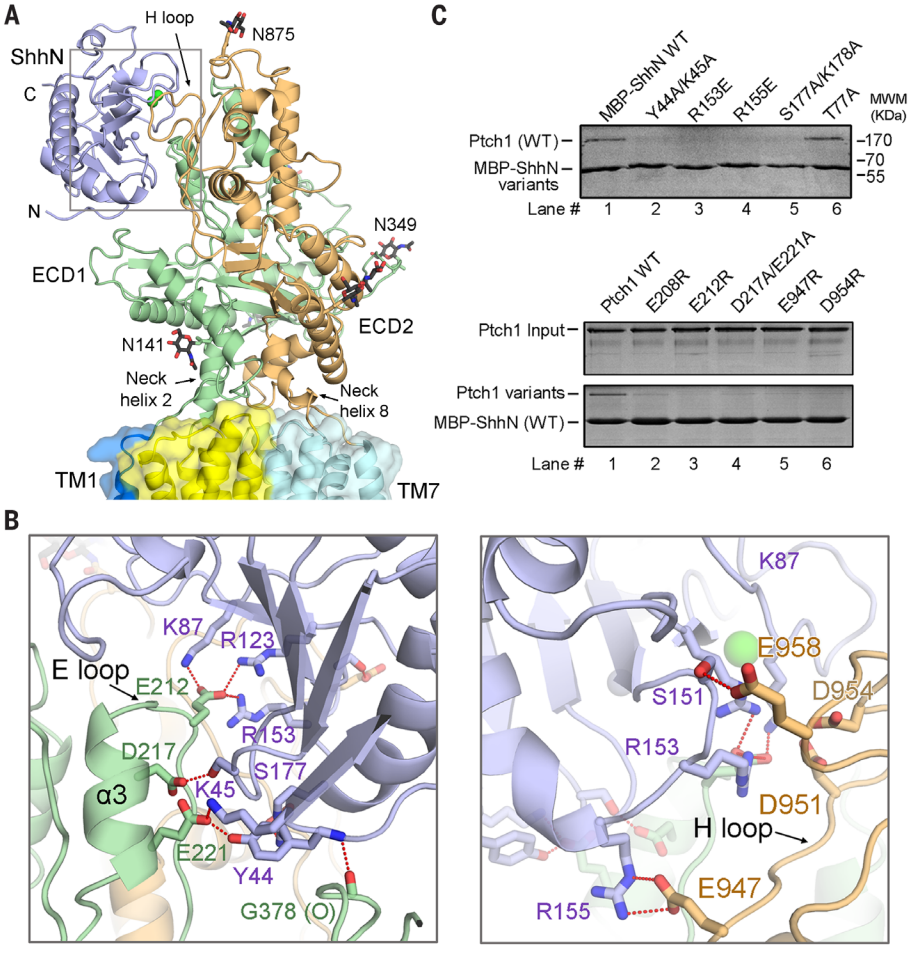

Fig. 2. Specific recognition between Ptch1 and ShhN. (**A**) The two extracellular domains, ECD1 and ECD2, of Ptch1 together constitute the docking site for ShhN. (**B**) The ECDs of Ptch1 recognize ShhN through extensive polar interactions. The left and right panels highlight the specific recognition of ShhN by ECD1 and ECD2, respectively. The potential electrostatic interactions are represented by dotted red lines. (**C**) Biochemical verification of the observed interface.

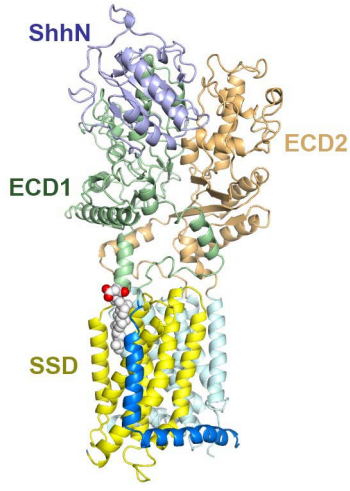

Movie 1. Conformational changes of Ptch1 upon ShhN binding. The morph was generated using the ShhN-free and -bound structures of Ptch1 as the first and end frames. The structures are shown as cartoon and domain-colored. The morph was generated by aligning the two structures and generating 60 intermediates in Chimera. The morphs were merged and displayed in PyMol using the "mset" command.

the ECDs, whereas the transmembrane segments remain unchanged (Movie 1). The two ECDs, which exhibit limited intradomain rearrangements except for some loop regions, move toward each other upon ShhN binding, resulting in increased interface between ECD1 and ECD2 from ~3830 Å^2 to ~4370 Å^2 (Fig. 3A). Helix α1, which connects to TM1 via linker 1, swings together with ECD2 (Fig. 3A, left). The lengthy linker 1 and the C-terminal short loop that connect the Neck helix to the TMD may confer the structural plasticity for the observed domainwise swing motions. Note that whereas the residues in the E loop in ECD1 are well resolved in the Ptch1-ShhN complex, even the backbone of the corresponding segment is broken in the map for Ptch1 alone, which suggests that this segment is stabilized by ShhN (Fig. 3B).

In addition to accommodating ShhN, the E loop covers a pocket on the interface of ECD1 and ECD2. Unexpectedly, a stretch of density is observed in this elongated pocket in both EM reconstructions with or without ShhN (Fig. 3, C and D, and fig. S6D). In the EM map for the Ptch1-ShhN complex (3.6 Å resolution), the density sealed between ECD1 and ECD2 is better defined and has a size and shape consistent with a cholesteryl hemisuccinate (CHS) molecule. The CHS molecule is localized on the interface between the upper helical domains of the two ECDs, where ECD1 provides the primary coordination. Nearly 20 hydrophobic residues on the E loop and helices α3, α6, and α7 from ECD1 form the contour of the pocket for CHS, whereas ECD2 only engages two small hydrophobic residues, Val^{932} and Ala^{935}, on its helix α7 (Fig. 3D).

Although CHS appears to be sealed within the ECDs, it was in the buffer used for protein extraction, suggesting dynamic access to this extracellular steroid-binding site (ESBS). As the E loop and helix α3 on ECD1 are also the major constituents of the docking site for ShhN (Fig. 2B),

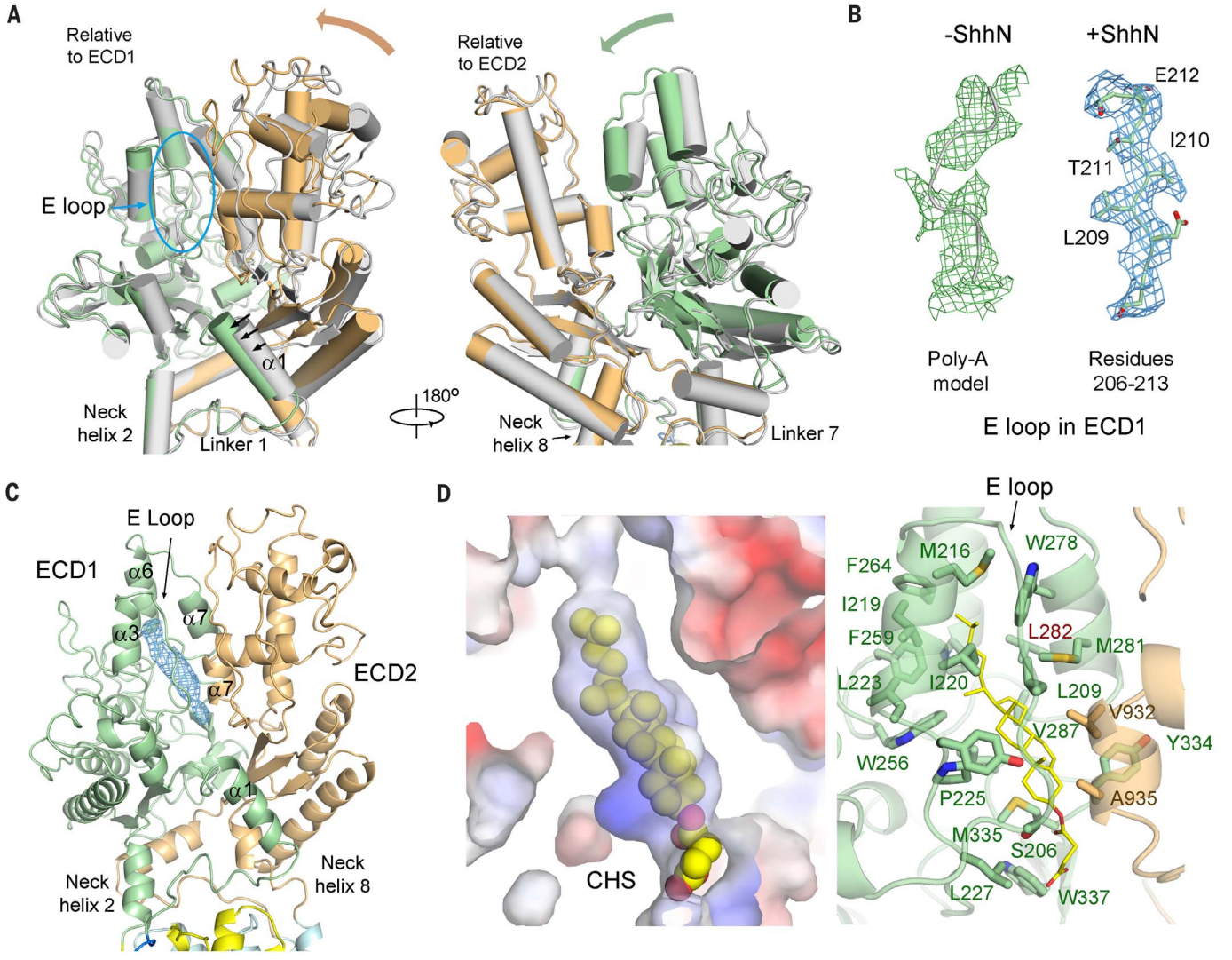

Fig. 3. The extracellular steroid-binding site (ESBS) is sealed upon ShhN binding. (**A**) The two ECDs of Ptch1 close up upon ShhN binding. The structural comparison of Ptch1 in the absence (silver) and presence (domain-colored) of ShhN is made relative to ECD1 (left) and ECD2 (right). See Movie 1 for the morph illustrating the conformational changes of Ptch1 upon ShhN association. (**B**) The E loop in ECD1 appears to be stabilized by ShhN. Shown here are the local EM maps, both contoured at 5σ, for the E loop in Ptch1 alone (left) and in the presence of ShhN (right). (**C**) A CHS-like density is embedded in the cavity enclosed by ECD1 and ECD2 in Ptch1. Shown here is the density in the Ptch1-ShhN complex. For the corresponding density in Ptch1 alone, see fig. S6D. (**D**) ECD1 provides the primary accommodation site for the CHS molecule. Left: The contour and composition of the cavity define the orientation of the bound CHS. Shown here is a cut-open view of the electrostatic surface potential of Ptch1 in the complex. CHS is shown as yellow spheres. Right: The E loop and helix α3 in ECD1 and helix α7 in ECD2 serve as the lid that shields the ligand. The residues that constitute the pocket are shown as sticks. Note that a cholesterol molecule can be accommodated in the hydrophobic pocket the same as CHS.

the different quality of the EM maps for this region with or without ShhN suggests that binding of ShhN may restrict the motion of these gating elements, hence potentially limiting the access to or exit from the ESBS.

Coordination of the steroidal moiety by the SSD

A similar stretch of density is found in a surface cavity on the membrane-facing side of the SSD. Although the size and shape of the density are also consistent with a CHS, we cannot exclude the possibility that it may belong to an endogenous molecule or a digitonin (Fig. 4A). The hydrophobic composition and the V shape of the SSD cavity define the orientation of the bound ligand. We modeled a CHS molecule into the density. A number of conserved hydrophobic residues on TMs 2 to 4 of the SSD shape the cavity that accommodates the cholesteryl moiety (Fig. 4A, insets, and fig. S9).

Although the ligand seems to bind to a similar location as the computationally predicted docking site on the SSD of NPC1 (*45*), the exact position and detailed coordination may be different. The SSDs exhibit considerable conformational divergence between Ptch1 and NPC1 (Fig. 4B). In both proteins, a well-characterized Pro residue (Pro^{691} in NPC1 and Pro^{504} in Ptch1) maps to the bottom of the SSD pocket and directly participates in the ligand interaction (Fig. 4C and fig. S9A). The single point mutation $Pro^{691} \rightarrow$ Ser, which is a disease mutation associated with Niemann-Pick disease type C, was shown to eliminate the cross-linking of NPC1 with the compound U18666A, a steroid blocker for NPC1-mediated cholesterol egress (*54*). Ptch1-P504L ($Pro^{504} \rightarrow$ Leu) is associated with Gorlin syndrome (*55*). Structural analysis of Ptch1 suggests that substitution of the Pro with a polar residue (Ser) or a bulky residue (Leu) may alter the chemical environment or change the contour of the pocket, hence making it less favorable for accommodating a cholesteryl moiety (Fig. 4, A and C).

The interaction between ShhN and Ptch1 is ligand-dependent

To validate the structural observations and to investigate the functional relevance of the bound steroid ligands, we generated three Ptch1 variants with point mutations designed to disrupt

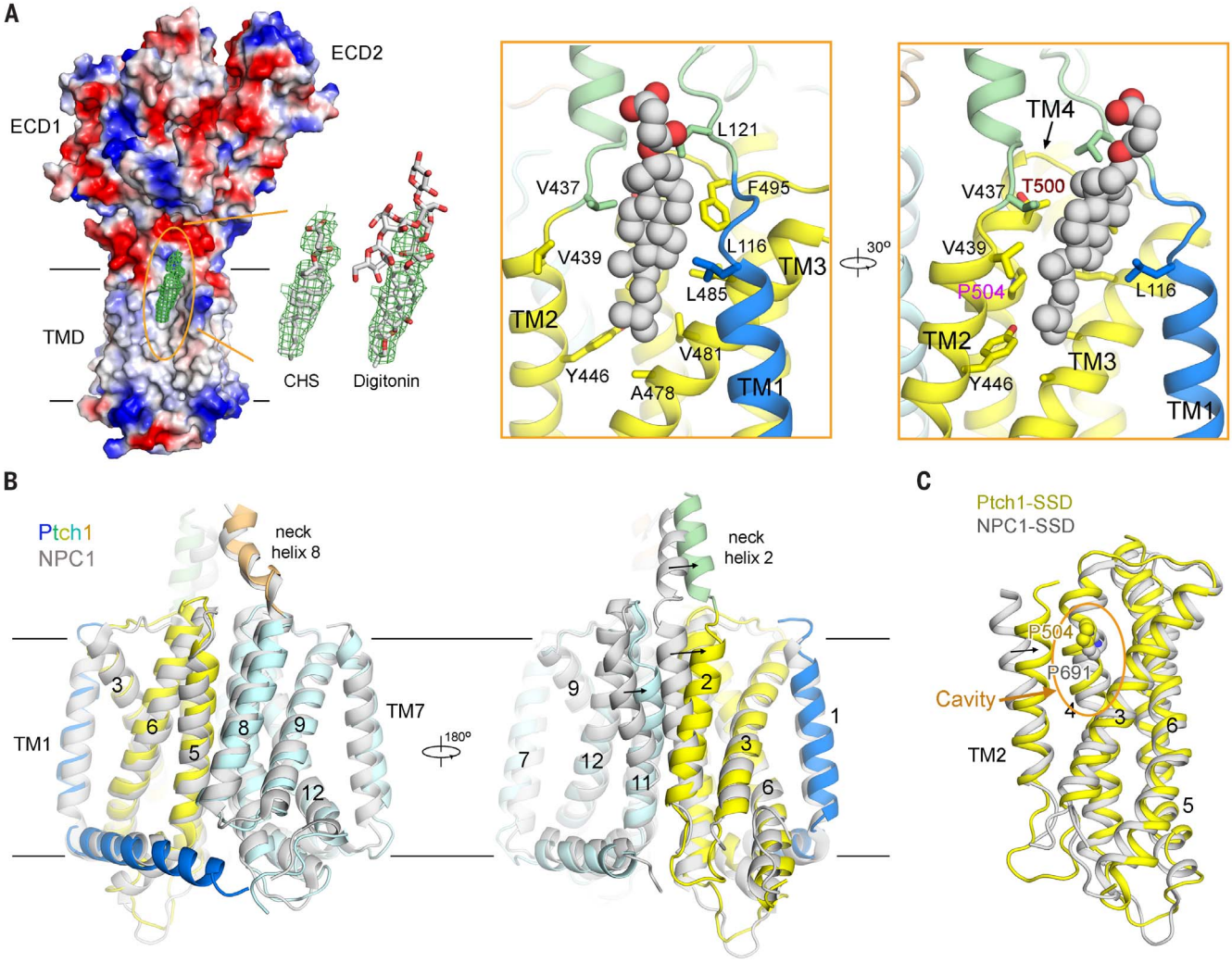

Fig. 4. Coordination of the cholesteryl moiety by the sterol-sensing domain (SSD). (**A**) The cavity on the membrane-facing side of SSD can accommodate a cholesterol-like molecule. The density is consistent with a CHS molecule, although the steroidal backbone of digitonin can fit in the density in a less favorable manner. Insets: Coordination of the cholesteryl moiety by SSD residues. Hydrophobic residues on TMs 2 to 4 of SSD constitute a V-shaped cavity, defining the orientation of the ligand should it be a cholesterol or cholesteryl derivative. Note that the hemisuccinate group of CHS is not specifically coordinated. Therefore, the observed interactions would be the same for a cholesterol molecule. (**B**) Structural comparison of the TMDs of Ptch1 and NPC1 (PDB code 5U74). TM2, TM11, and Neck helix 2 exhibit pronounced conformational changes between Ptch1 and NPC1. (**C**) Conformational divergence of the SSD between Ptch1 and NPC1. Ptch1-TM2 moves toward TM3, resulting in a narrower SSD cavity relative to that in NPC1-SSD. Within the cavity, a conserved and functionally important Pro (Pro^{691} in NPC1, Pro^{504} in Ptch1) is mapped to the side wall.

steroid binding: Ptch1-L282Q (Leu^{282} → Gln), where the hydrophobic residue within the ESBS is replaced by a polar one (Fig. 3D); Ptch1-T500F/P504L (Thr^{500} → Phe and Pro^{504} → Leu), in which the substitution with bulky residues may interfere with steroid binding to the SSD (Fig. 4A, right inset); and Ptch1-3M (with all three of these point mutations). It is difficult to directly measure the affinities between steroid molecules and the Ptch1 variants because of the interference by the detergent micelles. We therefore sought to solve the structures of Ptch1 variants using protocols identical to those for wild-type proteins.

Because the Ptch1-ShhN complex exhibits better resolution, we had planned to solve the structure of the complex. However, complex formation was markedly compromised between ShhN and all three Ptch1 variants. In particular, Ptch1-3M could be pulled down only minimally by MBP-ShhN (Fig. 5A). To semiquantitatively compare the affinity with ShhN between these variants and Ptch1-WT, we performed a concentration gradient titration of Ptch1 proteins (Fig. 5B). The affinity for ShhN of the ESBS mutant L282Q and the SSD mutant T500F/P504L appeared to be weakened by factors of approximately 16 and 4, respectively, whereas that of Ptch1-3M was reduced by more than a factor of 64. This observation seems to suggest a synergistic effect on the interaction with ShhN by the two steroid-binding sites (Fig. 5B).

To validate that the reduced ShhN binding was indeed related to steroid binding, we next examined the effect of CHS on complex formation (Fig. 5C). Ptch1 purified with *n*-dodecyl-β-D-maltopyranoside (DDM) barely interacted with ShhN, whereas addition of CHS restored complex formation (Fig. 5C, lanes 1 and 2). CHS was also required for ShhN binding when Ptch1 was purified with the detergents $C_{12}E_8$ or Cymal-6, which have distinct polar and hydrophobic moieties (Fig. 5C, lanes 3 to 6). In contrast, digitonin was sufficient to support complex formation (Fig. 5C, lane 7).

Taken together, our biochemical analyses suggest that complex formation between ShhN and Ptch1 may depend on the steroid ligand. To elucidate the molecular basis for this biochemical discovery, we focused on the structural determination of Ptch1-3M.

Pronounced conformational changes of Ptch1 upon steroid binding

The protocol for purification and data collection of Ptch1-3M is identical to that of Ptch1-WT. The numbers of the initial (>3.3 million) and selected (154,721) particles for 3D map reconstruction were both higher than that for Ptch1-WT alone and in complex with ShhN (Table 1); however, the final resolution was 4.1 Å for the overall structure of Ptch1-3M (figs. S4C, S5A, and S10A). As anticipated, the densities corresponding to CHS in the ESBS and SSD diminished, confirming the disrupted steroid binding by these point mutations (Fig. 6A).

Surprisingly, the overall structure of Ptch1-3M undergoes striking rearrangements from that of the wild-type protein (Movie 2). When the two structures are overlaid relative to the SSD, both TMD1/2 and ECD1/2 undergo marked twists (Fig. 6B). Individual domain comparison shows minor interdomain shifts between the two ECDs (Fig. 6C and Movie 2). Within ECD1, the E loop, whose backbone exhibits broken density in Ptch1-WT alone (Fig. 3B), is invisible in Ptch1-3M, indicating increased flexibility in the absence of CHS (Fig. 6A). Meanwhile, helix α3 moves toward the pocket (Fig. 6C). The resolution of the ECDs in Ptch1-3M is also considerably lower than that in Ptch1-WT (fig. S10), suggesting increased overall mobility. Because ECD1 and ECD2 need to move closer to form the ShhN docking site (Fig. 3A), the increased flexibility of the ECDs, particularly of the E loop and helix α3, may account for the reduced binding affinity with ShhN when the ESBS is not occupied by a steroid ligand.

Structural comparison of Ptch1-3M and Ptch1-WT affords an opportunity to investigate how the SSD senses sterol. Because none of the three residues Leu^{282}, Thr^{500}, or Pro^{504} is involved in intraprotein interaction, the structural shifts from Ptch1-3M (steroid-free) to Ptch1-WT (steroid-bound) may be interpreted as the conformational changes induced by arrival of the steroid ligand.

Binding of the steroid molecule to the SSD causes Neck helix 2, TM2, and TM4 to tilt toward the ligand (Fig. 6, D and E, and Movie 2). Such conformational shifts are similar to those observed in the structural comparison between ligand-free NPC1 and Ptch1-WT (Fig. 4, B and C). However, the pronounced relative rotation of the two TMDs around an axis that is perpendicular to their interface is unexpected (Fig. 6D, left, and Movie 2). Detailed structural comparison of Ptch1-3M and Ptch1-WT reveals the interdomain interactions that underlie the coupled conformational changes of TMD1/2 and ECD1/2 (Fig. 6, B and D, and Movie 3).

The short linker between TM5 and TM6 shifts concertedly with TM4 upon steroid binding (Fig. 6E) and pulls along linker 1 and helix α1 in ECD1. The motion of helix α1 induces the domainwise motion of ECD2 (Fig. 6C and Movie 3). The two base domains and the short linker between TM11 and TM12 move concomitantly with Neck helix 2 through extensive interactions (Movie 3).

The coupled movements of the four domains, TMD1/2 and ECD1/2, predict that mutations in one domain may alter an event in another domain through allosteric action. Supporting this notion, lack of steroid binding to SSD may result in increased flexibility of the two ECDs, hence leading to reduced ShhN binding (Fig. 5, A and B). In addition, Ptch1 variants containing a single point mutation—G509V (Gly^{509} → Val) or D513Y

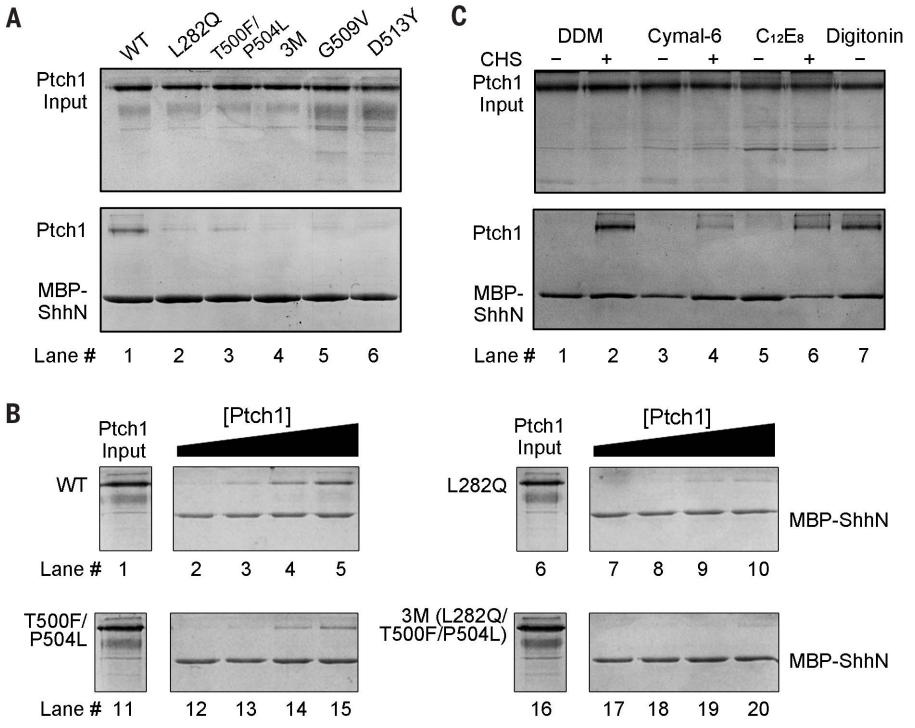

Fig. 5. SSD and ESBS mutations lead to reduced ShhN binding. (**A**) Point mutations in SSD or ESBS that are designed to disrupt steroid binding lead to reduced ShhN affinity. 3M denotes the Ptch1 variant containing L282Q, T500F, and P504L point mutations. (**B**) Concentration titration of Ptch1 variants in the pull-down assay semiquantitatively reveals the distinct effect of SSD and ESBS mutations on ShhN binding. (**C**) The interaction between purified Ptch1 and ShhN appears to be steroid-dependent. Ptch1 was purified in distinct detergents as indicated. CHS is required to retain the interaction when DDM, Cymal-6, or $C_{12}E_8$ was used for Ptch1 purification. Ptch1 purified in digitonin forms a complex with ShhN in the absence of CHS.

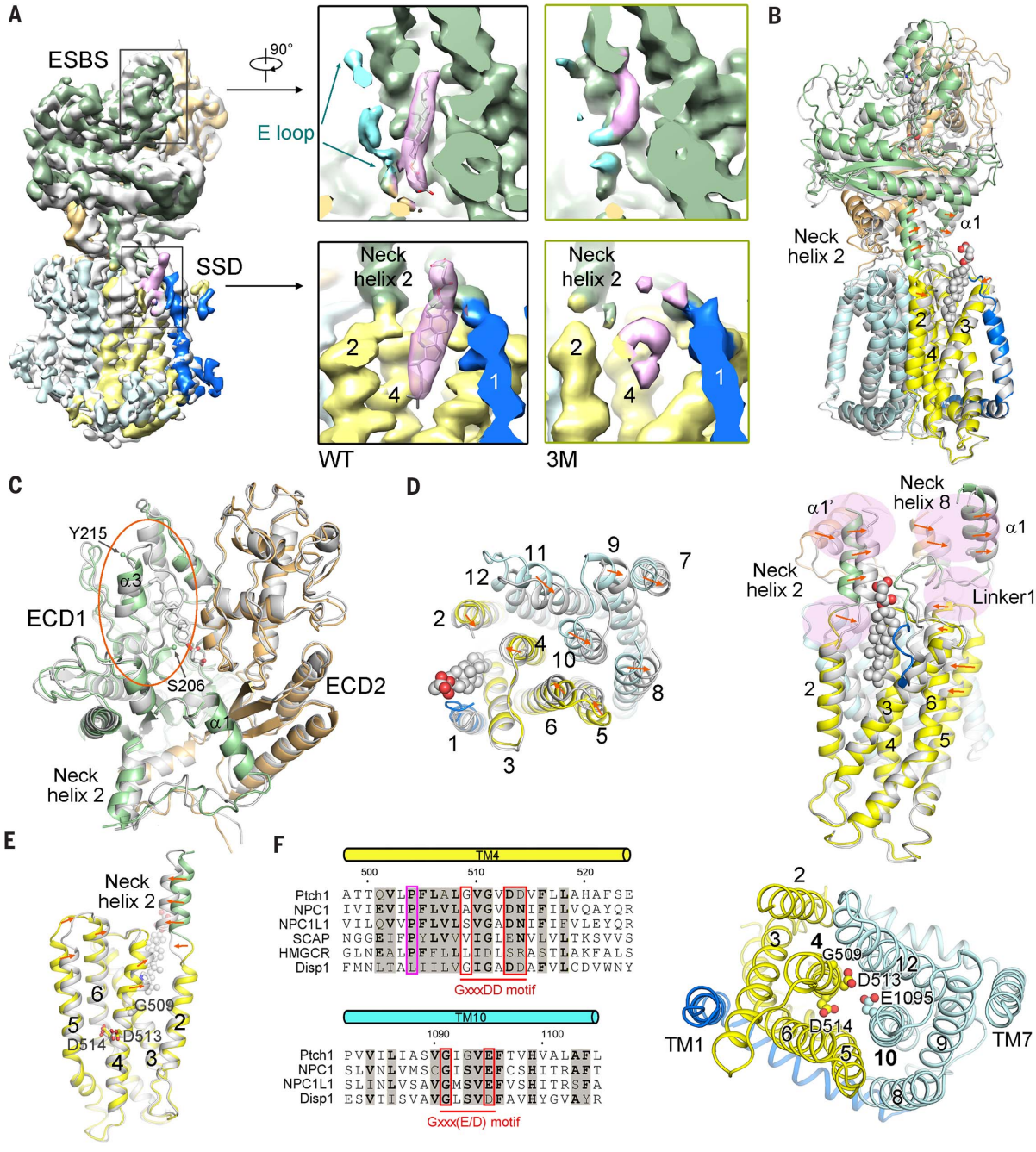

Fig. 6. Marked conformational changes of Ptch1 upon CHS binding. (**A**) Comparison of the EM maps of Ptch1-WT (silver) and Ptch1-3M (domain-colored). Both EM maps are low-pass filtered to 4.1 Å. The densities corresponding to the ligands in ESBS and SSD largely disappeared in the EM map of Ptch1-3M. Insets: The densities for CHS in ESBS (upper) and SSD (lower) are shown as semi-transparent contour in the low-pass filtered map of Ptch1-WT (left panels). Only shattered density debris remains at the corresponding positions in the map of Ptch1-3M (right panels). The E loop in ECD1 is no longer visible in Ptch1-3M. (**B**) Pronounced structural changes between Ptch1-WT (silver) and Ptch1-3M (domain-colored). The structural superimposition is made relative to SSD. See Movie 2 for the morph illustrating the overall conformational changes between the two structures. (**C**) ECDs undergo minor interdomain shifts between Ptch1-WT and Ptch1-3M. The two structures are superimposed relative to ECD1. The E-loop (residues 207 to 214) is invisible and helix α3 inclines toward the ESBS pocket. (**D**) Structural changes of Ptch1-TMD upon CHS binding. An extracellular view and a tilted side view are shown. The orange arrows indicate the shifts of the corresponding segments from Ptch1-3M to Ptch1-WT when the structural superimposition is made relative to SSD. The interactions that may be responsible for the coupled motions of different domains are highlighted by semitransparent pink patches. See Movie 3 for the morph illustrating the concerted movements of TMD1/2 and ECD1/2. (**E**) Structural changes of each SSD segment upon CHS binding. TM4, which moves toward the ligand, harbors the GxxxDD motif. (**F**) The acidic residues that are important for cotransport activity of RND members are conserved in Ptch1. Left: Sequence alignment of TM4 and TM10 from the indicated human SSD-containing proteins. The conserved and functionally crucial Pro in TM4 is highlighted by magenta box. The GxxxDD motif on TM4 and the Gxxx(E/D) motif on TM10, whose corresponding residues are essential for ion flux in the bacterial RND family, are highlighted by red boxes. Right: The conserved acidic residues on TM4/10 of Ptch1 are clustered in the center of the interface between TMD1 and TMD2. Shown here is an extracellular view of the Ptch1-TMD.

(Asp^{513} → Tyr), both of which are severe oncogenic mutations associated with Gorlin syndrome (*56*–*58*)—also exhibited reduced ShhN binding (Fig. 5A, lanes 5 and 6). Gly^{509} and Asp^{513} are localized in the middle segment of TM4 and mapped to the interface with TMD2 (Fig. 6F). As TM4 provides the primary site for steroid binding to SSD, these point mutations on the TMD2-facing side of TM4 may trap Ptch1 in a conformation that is incompatible for steroid binding to its SSD.

Discussion

Structural implications for steroid perception by SSD

SSD-containing proteins are associated with cholesterol metabolism and transport (*43*). For instance, SCAP is a key player in the sterol regulatory element–binding protein (SREBP) pathway that controls the cellular homeostasis of sterol (*59*), HMGCR catalyzes the rate-limiting step of cholesterol synthesis (*60*), and NPC1 is essential for cholesterol egress from the lysosomes and late endosomes to other cellular compartments (*61*). However, direct evidence for sterol binding by the SSD has been missing. We find that Ptch1 possesses two sites that can accommodate steroid molecules, one within the ECDs and the other on the SSD.

Structural comparison of the ligand-free Ptch1-3M and CHS-bound Ptch1-WT reveals the conformational changes of the SSD as well as the overall structure upon CHS binding (Fig. 6). Also considering the structural differences of the SSDs between the ligand-free NPC1 and CHS-bound Ptch1 (Fig. 4C), the CHS-induced conformational changes observed here may represent a paradigm that SSD-containing proteins use for sterol perception.

Potential cross-talk between the ESBS and SSD

Although the steroid binding to the SSD was anticipated, the extracellular steroid-binding site in Ptch1 and the steroid-dependent binding between Ptch1 and ShhN were not. An immediate question concerns the source of this trapped steroid. Because of its highly hydrophobic nature, a free cholesterol would be unlikely to diffuse into this site directly from the aqueous milieu, unless it is a cholesterol derivative with increased water solubility. There are then three possible sources for a hydrophobic steroid molecule: (i) It may be delivered by a NPC2-like lipid transfer

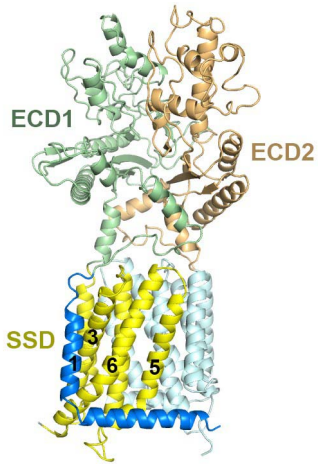

Movie 2. Conformational changes of Ptch1 upon CHS binding. The structures of Ptch1-3M and Ptch1-WT represent the starting and end frames. The procedure for morph generation was the same as for Movie 1.

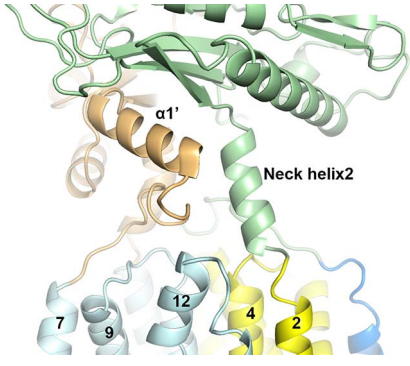

Movie 3. The coupled motions of distinct domains in Ptch1 upon CHS binding. The morph is the same as in Movie 2. The zoomed-in views highlight the interactions that may underlie the concerted motions of TMD1/2 and EMD1/2 upon CHS binding.

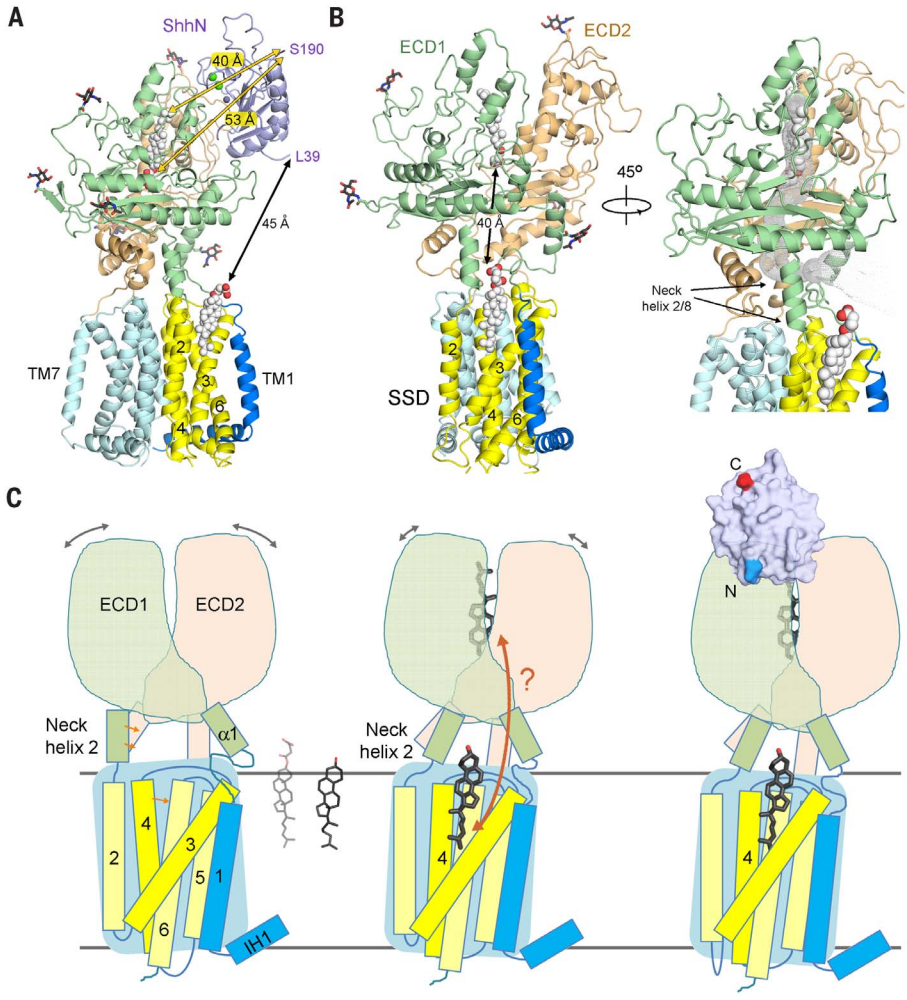

Fig. 7. Functional implications of the structures. (**A**) The relative positions of the two CHS molecules with respect to the N and C termini of ShhN in the complex. (**B**) The relative positions of the two steroid-binding sites on Ptch1. Right: ECD1 and ECD2 enclose a tunnel that can access to both ESBS and SSD. The tunnel is calculated by HOLE (*82*). (**C**) Summary of the structures reported in this study. Cartoons highlight the differences in the structures of Ptch1-3M (left), Ptch1-WT alone (center), and Ptch1-ShhN complex (right). The gray double-headed arrows indicate the structural flexibility of the ECDs. The same views of a CHS (gray) and a cholesterol (black) are shown to indicate their identical backbone. The physiologically relevant cholesterol is shown in the structural model. See text for discussion of functional implications of the structures.

protein, (ii) it may come from a steroidal moiety on a posttranslationally modified protein, or (iii) it may be extracted from the membrane and transferred to the ESBS by Ptch1 itself.

Although option 1 is formally possible, there has been no report on extracellular lipid-transfer proteins for Ptch1. With respect to option 2, the C-terminal Gly^{197} of ShhN is modified by a cholesteryl moiety, which can be a potential source. However, the last visible residue on the C terminus of ShhN is Ser^{190}, and a seven-residue peptide, even in a completely extended conformation, is not long enough to deliver the cholesteryl moiety to the ESBS in cis (Fig. 7A). In addition, in the structure of Ptch1 alone, the ESBS may allow a peptide to be connected to the steroid ligand; however, the sealed ESBS can hardly accommodate such a peptide in the Ptch1-ShhN complex (Fig. 7A). Therefore, we do not favor possibility 2.

Ptch1 has been speculated to be a transporter given its structural similarity with the RND pumps (*9*). A recent study discovered that Ptch1-mediated inhibition of Smo depends on extracellular Na^+ (*62*). Furthermore, the GxxxD(D) motif on TM4 and similar Gxxx(E/D) motif on TM10, which are required for the cotransport activity of the bacterial RND transporters, are conserved in Ptch1 (Fig. 6, E and F) (*9*, *63*). Consistent with steroid transport, ECD1 and ECD2 of Ptch1 encompass a tunnel that connects the ESBS and SSD in the absence of ShhN (Fig. 7B). It remains to be investigated whether a steroid molecule can be transferred between these two sites, and if so, whether this tunnel provides the diffusion path (Fig. 7C).

Structural implications for Hh signaling

Despite decades of rigorous characterization, the molecular mechanism for the inhibition of Smo by Ptch1 and the release of the inhibition by ShhN remains enigmatic. There are several outstanding questions. For instance, if Ptch1 functions as a sterol transporter, the transport activity is yet to be established. In addition, the abundance of cholesterol or its derivatives in primary cilia where Ptch1 inhibits Smo is unclear (*64*). Despite these and other outstanding questions, the three structures presented here reveal that Ptch1 undergoes steroid-induced conformational changes while binding of ShhN locks Ptch1 in one conformation (Fig. 7C). These findings lead us to speculate that the steroid-dependent structural shifts of Ptch1 may be required for its suppression of Smo, and that ShhN may inhibit Ptch1 by blocking this conformational change.

Many fundamental questions remain with regard to the function and mechanism of Ptch1 and ShhN. For instance, the unpalmitoylated ShhN used in this study is less active than the palmitoylated form in a cell-based assay by a factor of 30 to 40, although it retains high affinity with Ptch1 (*26*, *65*). What is more intriguing, a palmitoylated N-terminal 22-residue peptide was recently shown to activate Hh signaling in a cell-based assay (*66*), which cannot be explained by the three structures. Palmitoylate may interfere with the conformational changes or steroid-binding ability of Ptch1. Another question concerns the endogenous ligand or substrate for Ptch1. The composition and contour of the ESBS and the SSD cavity both allow accommodation of cholesterol with orientations similar to that of the CHS in the structure (Fig. 7A). Cholesterol derivatives with small-size modifications at C3-OH may also be compatible. The endogenous ligand(s) for Ptch1 may also act as agonists or antagonists for Smo. The structures reported here provide the basis for docking or simulation analysis that may facilitate the identification of such ligands. Finally, the structures of Ptch1 and ShhN presented here are both of monomers. The functional relevance of their oligomeric form remains unclear.

Despite these questions, the structures of human Ptch1 and its complex with ShhN set an important framework for future investigation of Hh signaling initiation and provide insight into the functional mechanism of SSD-containing proteins.

Materials and methods

Protein expression and purification

The complementary DNA of human Ptch1 (Uniprot: Q13635; residues 1 to 1305) was subcloned into the pCAG vector with an N-terminal FLAG tag and a C-terminal His_{10} tag. The Ptch1 mutants were generated with a standard 2-step PCR-based strategy. When the HEK293F cell density reached 2.0×10^6 cells per ml, the cells were transiently transfected with the expression plasmids and polyethylenimines (PEIs) (Polysciences). Approximately 1 mg of plasmids were premixed with 3 mg of PEIs in 50 ml of fresh medium for 15 to 30 min before application. For transfection, 50 ml of mixture was added to 1 liter of cell culture and incubated for 30 min. Transfected cells were cultured for 48 hours before harvest. For purification of WT Ptch1 and its variants, the HEK293F cells were collected and resuspended in the buffer containing 25 mM Tris pH 8.0, 150 mM NaCl, and protease inhibitor cocktails (Amresco). After sonication on ice, the membrane fraction was solubilized at 4°C for 2 hours with 1% (w/v) DDM (Anatrace) and 0.2% CHS (Anatrace). For biochemical assays reported in Fig. 5C, the protein was extracted using 1% (w/v) indicated detergents in the absence or presence of 0.2% CHS. After centrifugation at 20,000*g* for 1 hour, the supernatant was collected and applied to anti-Flag M2 affinity resin (Sigma). The resin was rinsed with wash buffer (W1 buffer) containing 25 mM Tris pH 8.0, 150 mM NaCl, 0.06% digitonin (w/v) (Sigma) or two critical micelle concentrations (CMC) of the other detergents with/without CHS as indicated in Fig. 5C, and protease inhibitors. The protein was eluted with W1 buffer plus FLAG peptide (200 μg/ml). The eluent was then applied to the nickel affinity resin (Ni-NTA, Qiagen). After three times of rinsing with W1 buffer plus 20 mM imidazole, the protein was eluted from the nickel resin with W1 buffer plus 250 mM imidazole. The eluent was then concentrated and further purified by SEC (Superose 6 10/300 GL, GE Healthcare) in buffer containing 25 mM Tris pH 8.0, 150 mM NaCl, and 0.06% digitonin or two CMC of the other detergents with/without CHS as indicated in Fig. 5C. Ptch1 proteins were eluted in two peaks, which were separately pooled and concentrated for EM and biochemical analysis. The later peak corresponding to monomer was pooled and concentrated to ~15 mg/ml for cryo sample preparation. The former peak corresponding to oligomer was used for the pull-down assay for different detergents as shown in Fig. 5C, whereas the latter peak was used for all the other pull-down assays.

The complementary DNA of human Shh (Uniprot: Q15465) N-terminal domain (ShhN, residues 24 to 197) was subcloned into the pET15 vector with N-terminal His_6 or MBP tags. The ShhN mutants were generated with a standard PCR-based strategy. The expression plasmids were transformed into *E. coli* BL21 (DE3) strain and protein overexpression was induced by 0.2 mM isopropyl β-D-thiogalactoside at an OD_{600nm} of 1.0. After growing at 20°C for 16 hours, the cells were collected and homogenized in buffer containing 25 mM Tris pH 8.0 and 150 mM NaCl. After sonication and centrifugation, the supernatant was applied to Ni-NTA affinity resin or amylose resin (New England Biolabs) and further purified by ion-exchange chromatography (Source 15S, GE Healthcare) and SEC (Superdex 200 10/300 GL, GE Healthcare). The peak fractions were pooled and concentrated for structural and biochemical analysis.

The Ptch1-ShhN complex was reconstituted by incubating the purified and concentrated Ptch1 and ShhN at a mass ratio of approximately 2:1 at 4°C for 1.5 hours before cryo-sample preparation.

Cryo-EM sample preparation and data collection

The cryo grids were prepared using Thermo Fisher Vitrobot Mark IV. The Quantifoil R1.2/1.3 Cu grids were glow-discharged with air for 30 s at medium level in Plasma Cleaner (Harrick Plasma, PDC-32G-2). Aliquots of 3.5 μl of purified Ptch1-WT, Ptch1-3M, or Ptch1-ShhN complex were applied to glow-discharged grids. After being blotted with filter paper for 4.0 s, the grids were plunged into liquid ethane cooled with liquid nitrogen. A total of 3983 micrograph stacks for Ptch1-WT, 6680 micrograph stacks for Ptch1-3M, and 4221 micrograph stacks for Ptch1-ShhN complex were automatically collected with AutoEMation II (*67*, *68*) on Titan Krios at 300 kV equipped with K2 Summit direct electron detector (Gatan), Quantum energy filter (Gatan), Cs corrector (Thermo Fisher), and Volta phase plate (Thermo Fisher) at a nominal magnification of 105,000× with a fixed defocus value of −0.7 μm. Each stack was exposed in super-resolution mode for 5.6 s with an exposing time of 0.175 s per frame, resulting in 32 frames per stack. The total dose rate was about 50 $e^-/Å^2$ for each stack. The stacks were first motion-corrected with MotionCorr (*69*) and binned 2-fold, resulting in a pixel size of 1.091 Å/pixel.

The output stacks from MotionCorr were further motion-corrected with MotionCor2 (*70*); meanwhile, dose weighting was performed (*71*). The defocus values were estimated with Gctf (*72*).

Cryo-EM data processing

For the Ptch1-WT dataset, a total of 1,710,446 particles were automatically picked with RELION 2.0 (*73*). After 2D classification, a 3D initial model was built from typical 2D class averages with e2initialmodel.py (*74*). A total of 736,934 particles were selected from 2D classification and subjected to a global angular search 3D classification with one class and 40 iterations. The outputs of the 33rd to 40th iterations were subjected to local angular search 3D classification with four classes separately. A total of 516,223 particles were selected by combining the good classes of the local angular search 3D classification, yielding a 3D reconstruction with an overall resolution of 6.1 Å after 3D auto-refinement. The handedness of the 3D reconstruction was checked and corrected. Then 156,723 particles were selected after 3D classification against one good reference and four bad references, giving rise to improved resolution at 4.4 Å after 3D auto-refinement. Finally, a subset of 94,445 particles were further selected by "skip alignment" 3D classification with an adapted mask, yielding overall resolution of 3.9 Å after 3D auto-refinement. The procedure for data processing of the Ptch1-3M was the same as that for Ptch1-WT. Eventually a subset of 154,721 particles was selected to generate a 3D reconstruction with overall resolution of 4.1 Å.

The procedure for data processing of the Ptch1-ShhN complex was similar with that for Ptch1 alone. To be brief, 1,518,460 particles were automatically picked. 2D classification resulted in 716,512 good particles that were subjected to subsequent global angular search 3D classification and local angular search 3D classification. After combining the good classes, 435,942 particles yielded a 3D reconstruction with overall resolution of 5.6 Å. After 3D classification against one good reference and four bad references, 137,823 particles were selected and gave rise to a 3D reconstruction of 4.4 Å resolution, which was further improved to 3.6 Å by applying an adapted mask during 3D auto-refinement.

All 2D classification, 3D classification, and 3D auto-refinement were performed with RELION 2.0. Resolutions were estimated with the gold-standard Fourier shell correlation 0.143 criterion (*75*) with high-resolution noise substitution (*76*).

Model building and refinement

The Ptch1-ShhN complex map at 3.6 Å was used for de novo model building of Ptch1. A poly-Ala model was derived using the NPC1 structure as the initial model (PDB code 3JD8) in COOT (*77*). Sequence assignment was guided mainly by bulky residues such as Phe, Tyr, Trp, and Arg. The chemical properties of amino acids were taken into consideration to facilitate model building. The glycosylation sites predicted in UniProt were used for model validation. One or two N-acetylglucosamine moieties were built to each site based on the densities. The crystal structure of ShhN (PDB code 4C4M) was docked into the map for Ptch1-ShhN complex and adjusted manually in COOT. For the Ptch1-WT and Ptch1-3M, the structural model of Ptch1 from the complex was fitted into the corresponding maps followed by manual adjustment.

All structure refinements were carried out by PHENIX (*78*) in real space with secondary structure and geometry restraints. Overfitting of the models was monitored by refining the model against one of the two independent half-maps and testing the refined model against the other map (*79*).

MBP-mediated pull-down assay

For pull-down assays, the Ptch1 and MBP-ShhN, WT or indicated variants, were incubated with amylose resin resuspended in 200 μl of buffer containing 25 mM Tris pH 8.0, 150 mM NaCl, and 0.06% digitonin or the indicated detergents at concentration of their respective 2× CMC at 4°C for ~1 hour. Then the mixture was spun down at 500*g* for 3 min. After removing the supernatant, the resin was extensively rinsed with the assay buffer to remove unbound proteins. Finally the resin was resuspended in 200 μl of buffer, out of which 20 μl was applied to SDS-PAGE analysis followed by Coomassie blue staining.

In the assay reported in Fig. 3C, all the indicated Ptch1 and MBP-ShhN variants were applied at concentrations of ~0.15 mg/ml. In the titration pull-down assay reported in Fig. 5B, ShhN was used at ~0.15 mg/ml, while Ptch1 was serially diluted fourfold at concentrations of ~0.60, ~0.15, ~0.04, and ~0.01 mg/ml, respectively. In the assay to test the effects of different detergents on the complex formation, the molar ratio of the two proteins was approximately 1:1 with Ptch1 and MBP-ShhN at concentrations of ~0.15 and 0.08 mg/ml, respectively.

REFERENCES AND NOTES

1. J. Briscoe, P. P. Thérond, The mechanisms of Hedgehog signalling and its roles in development and disease. *Nat. Rev. Mol. Cell Biol.* **14**, 416–429 (2013). doi: 10.1038/nrm3598; pmid: 23719536
2. E. Pak, R. A. Segal, Hedgehog Signal Transduction: Key Players, Oncogenic Drivers, and Cancer Therapy. *Dev. Cell* **38**, 333–344 (2016). doi: 10.1016/j.devcel.2016.07.026; pmid: 27554855
3. P. W. Ingham, Y. Nakano, C. Seger, Mechanisms and functions of Hedgehog signalling across the metazoa. *Nat. Rev. Genet.* **12**, 393–406 (2011). doi: 10.1038/nrg2984; pmid: 21502959
4. L. Lum, P. A. Beachy, The Hedgehog response network: Sensors, switches, and routers. *Science* **304**, 1755–1759 (2004). doi: 10.1126/science.1098020; pmid: 15205520
5. P. W. Ingham, A. P. McMahon, Hedgehog signaling in animal development: Paradigms and principles. *Genes Dev.* **15**, 3059–3087 (2001). doi: 10.1101/gad.938601; pmid: 11731473
6. V. Marigo, R. A. Davey, Y. Zuo, J. M. Cunningham, C. J. Tabin, Biochemical evidence that patched is the Hedgehog receptor. *Nature* **384**, 176–179 (1996). doi: 10.1038/384176a0; pmid: 8906794
7. D. M. Stone *et al*., The tumour-suppressor gene patched encodes a candidate receptor for Sonic hedgehog. *Nature* **384**, 129–134 (1996). doi: 10.1038/384129a0; pmid: 8906787
8. N. Fuse *et al*., Sonic hedgehog protein signals not as a hydrolytic enzyme but as an apparent ligand for patched. *Proc. Natl. Acad. Sci. U.S.A.* **96**, 10992–10999 (1999). doi: 10.1073/pnas.96.20.10992; pmid: 10500113
9. J. Taipale, M. K. Cooper, T. Maiti, P. A. Beachy, Patched acts catalytically to suppress the activity of Smoothened. *Nature* **418**, 892–897 (2002). doi: 10.1038/nature00989; pmid: 12192414
10. R. Rohatgi, L. Milenkovic, M. P. Scott, Patched1 regulates hedgehog signaling at the primary cilium. *Science* **317**, 372–376 (2007). doi: 10.1126/science.1139740; pmid: 17641202
11. K. C. Corbit *et al*., Vertebrate Smoothened functions at the primary cilium. *Nature* **437**, 1018–1021 (2005). doi: 10.1038/nature04117; pmid: 16136078
12. P. Aza-Blanc, F. A. Ramírez-Weber, M. P. Laget, C. Schwartz, T. B. Kornberg, Proteolysis that is inhibited by hedgehog targets Cubitus interruptus protein to the nucleus and converts it to a repressor. *Cell* **89**, 1043–1053 (1997). doi: 10.1016/S0092-8674(00)80292-5; pmid: 9215627
13. C. H. Chen *et al*., Nuclear trafficking of Cubitus interruptus in the transcriptional regulation of Hedgehog target gene expression. *Cell* **98**, 305–316 (1999). doi: 10.1016/S0092-8674(00)81960-1; pmid: 10458606
14. N. Méthot, K. Basler, Hedgehog controls limb development by regulating the activities of distinct transcriptional activator and repressor forms of Cubitus interruptus. *Cell* **96**, 819–831 (1999). doi: 10.1016/S0092-8674(00)80592-9; pmid: 10102270
15. J. Kim, M. Kato, P. A. Beachy, Gli2 trafficking links Hedgehog-dependent activation of Smoothened in the primary cilium to transcriptional activation in the nucleus. *Proc. Natl. Acad. Sci. U.S.A.* **106**, 21666–21671 (2009). doi: 10.1073/pnas.0912180106; pmid: 19996169
16. J. W. Yoon *et al*., Gene expression profiling leads to identification of GLI1-binding elements in target genes and a role for multiple downstream pathways in GLI1-induced cell transformation. *J. Biol. Chem.* **277**, 5548–5555 (2002). doi: 10.1074/jbc.M105708200; pmid: 11719506
17. X. Wen *et al*., Kinetics of hedgehog-dependent full-length Gli3 accumulation in primary cilia and subsequent degradation. *Mol. Cell. Biol.* **30**, 1910–1922 (2010). doi: 10.1128/MCB.01089-09; pmid: 20154143
18. C. C. Hui, S. Angers, Gli proteins in development and disease. *Annu. Rev. Cell Dev. Biol.* **27**, 513–537 (2011). doi: 10.1146/annurev-cellbio-092910-154048; pmid: 21801010
19. J. Taipale, P. A. Beachy, The Hedgehog and Wnt signalling pathways in cancer. *Nature* **411**, 349–354 (2001). doi: 10.1038/35077219; pmid: 11357142
20. P. A. Beachy, S. S. Karhadkar, D. M. Berman, Tissue repair and stem cell renewal in carcinogenesis. *Nature* **432**, 324–331 (2004). doi: 10.1038/nature03100; pmid: 15549094
21. L. L. Rubin, F. J. de Sauvage, Targeting the Hedgehog pathway in cancer. *Nat. Rev. Drug Discov.* **5**, 1026–1033 (2006). doi: 10.1038/nrd2086; pmid: 17139287
22. J. Xie *et al*., Activating Smoothened mutations in sporadic basal-cell carcinoma. *Nature* **391**, 90–92 (1998). doi: 10.1038/34201; pmid: 9422511
23. R. K. Mann, P. A. Beachy, Novel lipid modifications of secreted protein signals. *Annu. Rev. Biochem.* **73**, 891–923 (2004). doi: 10.1146/annurev.biochem.73.011303.073933; pmid: 15189162
24. J. A. Porter, K. E. Young, P. A. Beachy, Cholesterol modification of hedgehog signaling proteins in animal development. *Science* **274**, 255–259 (1996). doi: 10.1126/science.274.5285.255; pmid: 8824192
25. J. A. Porter *et al*., Hedgehog patterning activity: Role of a lipophilic modification mediated by the carboxy-terminal autoprocessing domain. *Cell* **86**, 21–34 (1996). doi: 10.1016/S0092-8674(00)80074-4; pmid: 8689684
26. R. B. Pepinsky *et al*., Identification of a palmitic acid-modified form of human Sonic hedgehog. *J. Biol. Chem.* **273**, 14037–14045 (1998). doi: 10.1074/jbc.273.22.14037; pmid: 9593755
27. P. M. Lewis *et al*., Cholesterol modification of sonic hedgehog is required for long-range signaling activity and effective modulation of signaling by Ptc1. *Cell* **105**, 599–612 (2001). doi: 10.1016/S0092-8674(01)00369-5; pmid: 11389830
28. Z. Chamoun *et al*., Skinny hedgehog, an acyltransferase required for palmitoylation and activity of the hedgehog signal. *Science* **293**, 2080–2084 (2001). doi: 10.1126/science.1064437; pmid: 11486055
29. K. P. Williams *et al*., Functional antagonists of sonic hedgehog reveal the importance of the N terminus for activity. *J. Cell Sci.* **112**, 4405–4414 (1999). pmid: 10564658
30. B. Z. Stanton, L. F. Peng, Small-molecule modulators of the Sonic Hedgehog signaling pathway. *Mol. Biosyst.* **6**, 44–54 (2010). doi: 10.1039/B910196A; pmid: 20024066

31. S. Peukert, K. Miller-Moslin, Small-molecule inhibitors of the hedgehog signaling pathway as cancer therapeutics. *ChemMedChem* **5**, 500–512 (2010). doi: 10.1002/cmdc.201000011; pmid: 20229564
32. B. Z. Stanton *et al*., A small molecule that binds Hedgehog and blocks its signaling in human cells. *Nat. Chem. Biol.* **5**, 154–156 (2009). doi: 10.1038/nchembio.142; pmid: 19151731
33. A. E. Owens *et al*., Design and Evolution of a Macrocyclic Peptide Inhibitor of the Sonic Hedgehog/Patched Interaction. *J. Am. Chem. Soc.* **139**, 12559–12568 (2017). doi: 10.1021/jacs.7b06087; pmid: 28759213
34. P. A. Beachy, S. G. Hymowitz, R. A. Lazarus, D. J. Leahy, C. Siebold, Interactions between Hedgehog proteins and their binding partners come into view. *Genes Dev.* **24**, 2001–2012 (2010). doi: 10.1101/gad.1951710; pmid: 20844013
35. J. E. Hooper, M. P. Scott, The Drosophila patched gene encodes a putative membrane protein required for segmental patterning. *Cell* **59**, 751–765 (1989). doi: 10.1016/0092-8674(89)90021-4; pmid: 2582494
36. Y. Nakano *et al*., A protein with several possible membrane-spanning domains encoded by the Drosophila segment polarity gene patched. *Nature* **341**, 508–513 (1989). doi: 10.1038/341508a0; pmid: 2797178
37. R. L. Johnson *et al*., Human homolog of patched, a candidate gene for the basal cell nevus syndrome. *Science* **272**, 1668–1671 (1996). doi: 10.1126/science.272.5268.1668; pmid: 8658145
38. H. Hahn *et al*., Mutations of the human homolog of Drosophila patched in the nevoid basal cell carcinoma syndrome. *Cell* **85**, 841–851 (1996). doi: 10.1016/S0092-8674(00)81268-4; pmid: 8681379
39. D. Carpenter *et al*., Characterization of two patched receptors for the vertebrate hedgehog protein family. *Proc. Natl. Acad. Sci. U.S.A.* **95**, 13630–13634 (1998). doi: 10.1073/pnas.95.23.13630; pmid: 9811851
40. P. G. Zaphiropoulos, A. B. Undén, F. Rahnama, R. E. Hollingsworth, R. Toftgård, PTCH2, a novel human patched gene, undergoing alternative splicing and up-regulated in basal cell carcinomas. *Cancer Res.* **59**, 787–792 (1999). pmid: 10029063
41. T. T. Tseng *et al*., The RND permease superfamily: An ancient, ubiquitous and diverse family that includes human disease and development proteins. *J. Mol. Microbiol. Biotechnol.* **1**, 107–125 (1999). pmid: 10941792
42. A. Yamaguchi, R. Nakashima, K. Sakurai, Structural basis of RND-type multidrug exporters. *Front. Microbiol.* **6**, 327 (2015). doi: 10.3389/fmicb.2015.00327; pmid: 25941524
43. P. E. Kuwabara, M. Labouesse, The sterol-sensing domain: Multiple families, a unique role? *Trends Genet.* **18**, 193–201 (2002). doi: 10.1016/S0168-9525(02)02640-9; pmid: 11932020
44. X. Gong *et al*., Structural Insights into the Niemann-Pick C1 (NPC1)-Mediated Cholesterol Transfer and Ebola Infection. *Cell* **165**, 1467–1478 (2016). doi: 10.1016/j.cell.2016.05.022; pmid: 27238017
45. X. Li *et al*., Structure of human Niemann-Pick C1 protein. *Proc. Natl. Acad. Sci. U.S.A.* **113**, 8212–8217 (2016). doi: 10.1073/pnas.1607795113; pmid: 27307437
46. M. C. Harvey, A. Fleet, N. Okolowsky, P. A. Hamel, Distinct effects of the mesenchymal dysplasia gene variant of murine Patched-1 protein on canonical and non-canonical Hedgehog signaling pathways. *J. Biol. Chem.* **289**, 10939–10949 (2014). doi: 10.1074/jbc.M113.514844; pmid: 24570001
47. A. Fleet, J. P. Lee, A. Tamachi, I. Javeed, P. A. Hamel, Activities of the Cytoplasmic Domains of Patched-1 Modulate but Are Not Essential for the Regulation of Canonical Hedgehog Signaling. *J. Biol. Chem.* **291**, 17557–17568 (2016). doi: 10.1074/jbc.M116.731745; pmid: 27325696
48. X. Lu, S. Liu, T. B. Kornberg, The C-terminal tail of the Hedgehog receptor Patched regulates both localization and turnover. *Genes Dev.* **20**, 2539–2551 (2006). doi: 10.1101/gad.1461306; pmid: 16980583
49. S. Murakami, R. Nakashima, E. Yamashita, A. Yamaguchi, Crystal structure of bacterial multidrug efflux transporter AcrB. *Nature* **419**, 587–593 (2002). doi: 10.1038/nature01050; pmid: 12374972
50. J. S. McLellan *et al*., The mode of Hedgehog binding to Ihog homologues is not conserved across different phyla. *Nature* **455**, 979–983 (2008). doi: 10.1038/nature07358; pmid: 18794898
51. B. Bishop *et al*., Structural insights into hedgehog ligand sequestration by the human hedgehog-interacting protein HHIP. *Nat. Struct. Mol. Biol.* **16**, 698–703 (2009). doi: 10.1038/nsmb.1607; pmid: 19561611
52. I. Bosanac *et al*., The structure of SHH in complex with HHIP reveals a recognition role for the Shh pseudo active site in signaling. *Nat. Struct. Mol. Biol.* **16**, 691–697 (2009). doi: 10.1038/nsmb.1632; pmid: 19561609
53. H. R. Maun *et al*., Hedgehog pathway antagonist 5E1 binds hedgehog at the pseudo-active site. *J. Biol. Chem.* **285**, 26570–26580 (2010). doi: 10.1074/jbc.M110.112284; pmid: 20504762
54. F. Lu *et al*., Identification of NPC1 as the target of U18666A, an inhibitor of lysosomal cholesterol export and Ebola infection. *eLife* **4**, e12177 (2015). doi: 10.7554/eLife.12177; pmid: 26646182
55. N. Boutet *et al*., Spectrum of PTCH1 mutations in French patients with Gorlin syndrome. *J. Invest. Dermatol.* **121**, 478–481 (2003). doi: 10.1046/j.1523-1747.2003.12423.x; pmid: 12925203
56. K. Fujii *et al*., Mutations in the human homologue of Drosophila patched in Japanese nevoid basal cell carcinoma syndrome patients. *Hum. Mutat.* **21**, 451–452 (2003). doi: 10.1002/humu.9132; pmid: 12655573
57. G. R. Hime *et al*., Functional analysis in Drosophila indicates that the NBCCS/PTCH1 mutation G509V results in activation of smoothened through a dominant-negative mechanism. *Dev. Dyn.* **229**, 780–790 (2004). doi: 10.1002/dvdy.10499; pmid: 15042702
58. G. Tate, M. Li, T. Suzuki, T. Mitsuya, A new germline mutation of the PTCH gene in a Japanese patient with nevoid basal cell carcinoma syndrome associated with meningioma. *Jpn. J. Clin. Oncol.* **33**, 47–50 (2003). doi: 10.1093/jjco/hyg005; pmid: 12604725
59. J. L. Goldstein, M. S. Brown, A century of cholesterol and coronaries: From plaques to genes to statins. *Cell* **161**, 161–172 (2015). doi: 10.1016/j.cell.2015.01.036; pmid: 25815993
60. K. L. Luskey, B. Stevens, Human 3-hydroxy-3-methylglutaryl coenzyme A reductase. Conserved domains responsible for catalytic activity and sterol-regulated degradation. *J. Biol. Chem.* **260**, 10271–10277 (1985). pmid: 2991281
61. M. T. Vanier, Complex lipid trafficking in Niemann-Pick disease type C. *J. Inherit. Metab. Dis.* **38**, 187–199 (2015). doi: 10.1007/s10545-014-9794-4; pmid: 25425283
62. B. R. Myers, L. Neahring, Y. Zhang, K. J. Roberts, P. A. Beachy, Rapid, direct activity assays for Smoothened reveal Hedgehog pathway regulation by membrane cholesterol and extracellular sodium. *Proc. Natl. Acad. Sci. U.S.A.* **114**, E11141–E11150 (2017). doi: 10.1073/pnas.1717891115; pmid: 29229834
63. L. Guan, T. Nakae, Identification of essential charged residues in transmembrane segments of the multidrug transporter MexB of Pseudomonas aeruginosa. *J. Bacteriol.* **183**, 1734–1739 (2001). doi: 10.1128/JB.183.5.1734-1739.2001; pmid: 11160105
64. S. C. Goetz, K. V. Anderson, The primary cilium: A signalling centre during vertebrate development. *Nat. Rev. Genet.* **11**, 331–344 (2010). doi: 10.1038/nrg2774; pmid: 20395968
65. F. R. Taylor *et al*., Enhanced potency of human Sonic hedgehog by hydrophobic modification. *Biochemistry* **40**, 4359–4371 (2001). doi: 10.1021/bi002487u; pmid: 11284692
66. H. Tukachinsky, K. Petrov, M. Watanabe, A. Salic, Mechanism of inhibition of the tumor suppressor Patched by Sonic Hedgehog. *Proc. Natl. Acad. Sci. U.S.A.* **113**, E5866–E5875 (2016). doi: 10.1073/pnas.1606719113; pmid: 27647915
67. J. Lei, J. Frank, Automated acquisition of cryo-electron micrographs for single particle reconstruction on an FEI Tecnai electron microscope. *J. Struct. Biol.* **150**, 69–80 (2005). doi: 10.1016/j.jsb.2005.01.002; pmid: 15797731
68. X. Fan *et al*., Near-Atomic Resolution Structure Determination in Over-Focus with Volta Phase Plate by Cs-Corrected Cryo-EM. *Structure* **25**, 1623–1630.e3 (2017). doi: 10.1016/j.jsb.2005.01.002; pmid: 15797731
69. X. Li *et al*., Electron counting and beam-induced motion correction enable near-atomic-resolution single-particle cryo-EM. *Nat. Methods* **10**, 584–590 (2013). doi: 10.1038/nmeth.2472; pmid: 23644547
70. S. Q. Zheng *et al*., MotionCor2: Anisotropic correction of beam-induced motion for improved cryo-electron microscopy. *Nat. Methods* **14**, 331–332 (2017). doi: 10.1038/nmeth.4193; pmid: 28250466
71. T. Grant, N. Grigorieff, Measuring the optimal exposure for single particle cryo-EM using a 2.6 Å reconstruction of rotavirus VP6. *eLife* **4**, e06980 (2015). doi: 10.7554/eLife.06980; pmid: 26023829
72. K. Zhang, Gctf: Real-time CTF determination and correction. *J. Struct. Biol.* **193**, 1–12 (2016). doi: 10.1016/j.jsb.2015.11.003; pmid: 26592709
73. D. Kimanius, B. O. Forsberg, S. H. Scheres, E. Lindahl, Accelerated cryo-EM structure determination with parallelisation using GPUs in RELION-2. *eLife* **5**, e18722 (2016). doi: 10.7554/eLife.18722; pmid: 27845625
74. G. Tang *et al*., EMAN2: An extensible image processing suite for electron microscopy. *J. Struct. Biol.* **157**, 38–46 (2007). doi: 10.1016/j.jsb.2006.05.009; pmid: 16859925
75. P. B. Rosenthal, R. Henderson, Optimal determination of particle orientation, absolute hand, and contrast loss in single-particle electron cryomicroscopy. *J. Mol. Biol.* **333**, 721–745 (2003). doi: 10.1016/j.jmb.2003.07.013; pmid: 14568533
76. S. Chen *et al*., High-resolution noise substitution to measure overfitting and validate resolution in 3D structure determination by single particle electron cryomicroscopy. *Ultramicroscopy* **135**, 24–35 (2013). doi: 10.1016/j.ultramic.2013.06.004; pmid: 23872039
77. P. Emsley, B. Lohkamp, W. G. Scott, K. Cowtan, Features and development of Coot. *Acta Crystallogr. D* **66**, 486–501 (2010). doi: 10.1107/S0907444910007493; pmid: 20383002
78. P. D. Adams *et al*., PHENIX: A comprehensive Python-based system for macromolecular structure solution. *Acta Crystallogr. D* **66**, 213–221 (2010). doi: 10.1107/S0907444909052925; pmid: 20124702
79. A. Amunts *et al*., Structure of the yeast mitochondrial large ribosomal subunit. *Science* **343**, 1485–1489 (2014). doi: 10.1126/science.1249410; pmid: 24675956
80. E. F. Pettersen *et al*., UCSF Chimera—a visualization system for exploratory research and analysis. *J. Comput. Chem.* **25**, 1605–1612 (2004). doi: 10.1002/jcc.20084; pmid: 15264254
81. W. L. DeLano, The PyMOL Molecular Graphics System; www.pymol.org. (2002).
82. O. S. Smart, J. G. Neduvelil, X. Wang, B. A. Wallace, M. S. Sansom, HOLE: A program for the analysis of the pore dimensions of ion channel structural models. *J. Mol. Graph.* **14**, 354–360 (1996). doi: 10.1016/S0263-7855(97)00009-X; pmid: 9195488

ACKNOWLEDGMENTS

We thank X. Li for technical support during EM image acquisition. **Funding:** Supported by National Key Basic Research (973) Program grant 2015CB910101 (N.Y.) and National Key R&D Program grants 2016YFA0500402 (N.Y.) and 2016YFA0501100 (J.L.) from Ministry of Science and Technology of China; National Natural Science Foundation of China projects 31621092, 31630017, and 31611130036 (N.Y.); and the Shirley M. Tilghman endowed professorship from Princeton University (N.Y.). We thank the Tsinghua University Branch of China National Center for Protein Sciences (Beijing) for providing cryo-EM facility support. We thank the computational facility support on the cluster of Bio-Computing Platform (Tsinghua University Branch of China National Center for Protein Sciences Beijing) and the "Explorer 100" cluster system of Tsinghua National Laboratory for Information Science and Technology. **Author contributions:** N.Y. and X.G. conceived the project; X.G., H.Q., P.C., X.Z., Q.Z., and J.L. performed the experiments; all authors contributed to data analysis; and N.Y. and X.G. wrote the manuscript. **Competing interests:** The authors declare no competing interests. **Data and materials availability:** Atomic coordinates and EM density maps of the human Ptch1-WT (PDB: 6DMB; EMDB: EMD-7963), Ptch1-3M (PDB: 6DMO; EMDB: EMD-7964), and ShhN-bound Ptch1 (PDB: 6DMY; EMDB: EMD-7968) have been deposited in the Protein Data Bank (www.rcsb.org) and the Electron Microscopy Data Bank (www.ebi.ac.uk/pdbe/emdb/).

SUPPLEMENTARY MATERIALS

www.sciencemag.org/content/361/6402/eaas8935/suppl/DC1
Figs. S1 to S10
References (*83*, *84*)

3 January 2018; accepted 19 June 2018
Published online 28 June 2018
10.1126/science.aas8935

Science

Structural basis for the recognition of Sonic Hedgehog by human Patched1

Xin Gong, Hongwu Qian, Pingping Cao, Xin Zhao, Qiang Zhou, Jianlin Lei and Nieng Yan

Science **361** (6402), eaas8935.
DOI: 10.1126/science.aas8935originally published online June 28, 2018

The first step in Hedgehog signaling

The Hedgehog (Hh) signaling pathway is important in embryogenesis; overactivation is associated with cancer. Central to the pathway is the membrane receptor Patched 1 (Ptch1), which indirectly inhibits a G protein–coupled receptor called Smoothened. This inhibition is relieved when Ptch1 binds the secreted protein Hh. Gong *et al.* report the cryo–electron microscopy structures of human Ptch1 alone and in complex with its Hh ligand at 3.9 and 3.6 Å, respectively. Both structures include two steroid-shaped densities, and mutational analysis indicates that the interaction between Ptch1 and Hh is steroid-dependent.

Science, this issue p. eaas8935